

Quasiharmonic periodic traveling-wave solutions in anharmonic potentials

A. Bussmann-Holder

Max-Planck-Institut für Festkörperforschung, Heisenbergstrasse 1, 70569 Stuttgart, Federal Republic of Germany

A. R. Bishop

Los Alamos National Laboratory, Theoretical Division, Los Alamos, New Mexico 87545

G. Benedek

Dipartimento di Fisica, Università di Milano, Via Celoria 16, 20133 Milano, Italy

(Received 17 August 1995; revised manuscript received 19 January 1996)

Exact solutions of a nonlinear diatomic shell model are investigated in the regime where quasiharmonic and pseudoperiodic traveling waves exist with phonon-type character. The existence regimes of these solutions are determined by the boundary conditions and the model parameters for which especially a strong time and mass dependence is observed. It is found that slowly propagating waves mostly show large displacement responses which can be associated with large dipole moments, while rapidly traveling waves carry a much smaller dipole moment, but still this is appreciably larger than that induced by bare optic-phonon modes. The case of large anharmonicity shows the opposite effect. Here high-frequency responses carry a large dipole moment. The large dipole moments can be associated with effective charges which induce high oscillator strengths in the corresponding phonon modes, incompatible with results deduced from harmonic lattice dynamics. The origin of the large dipole moments in the shell model is investigated by solving for core and shell displacements separately, where “acoustic-type” periodic in-phase displacements of core and shell with different amplitudes are observed, as well as pseudoperiodic out-of-phase “optic-type” displacements resulting from large anharmonicity, and are also found in the static limit. Besides the displacement frequency spectrum, the effective potentials are calculated which are distinctly different from ϕ_4 -type potentials: The potential height is finite with finite width which, in certain cases becomes very small, thus admitting for tunneling through the barrier.

I. INTRODUCTION

In a variety of recent work¹⁻⁴ a nonlinear shell model for structural instabilities related to ferro- and antiferroelectric phase transitions and local structural anomalies has been investigated. Three-dimensional⁵⁻¹⁰ as well as pseudo-one-dimensional versions¹¹⁻¹⁴ of this model have been used to calculate Raman spectra and infrared responses as well as the temperature dependences of soft modes and q dependences of the lattice modes. Excellent agreement with experimental data was achieved which demonstrates the value of phenomenologically derived models such as the shell model. The nonlinear shell model has been introduced in order to account for the highly nonlinear temperature- and volume-dependent polarizability of the oxygen ion¹⁵ which leads to a dynamical covalency. Clear confirmation of this phenomenology has been obtained recently from *ab initio* methods.^{16,17} As the phenomenological models exhibit high physical transparency, and since numerical calculations are much less expedient than using other methods, we continue here earlier work on exact solutions of the model.

The polarizability model is based on a ϕ_4 potential in the core-shell relative displacement. Using the adiabatic approximation for the shell equation of motion, it is possible to derive an effective potential for the relative displacement which exhibits qualitatively new features and solutions, as compared to the usual ϕ_4 or sine-Gordon-type models.¹⁸ Various solutions of this model have already been investigated in the lattice case,¹⁹⁻²¹ as well as in the continuum

limit.^{22,23} In the lattice case, periodic nonlinear waves have been discovered, which have been shown to model the antiferrodistortive-type phase transitions as observed, e.g., in K_2SeO_4 . In the continuum limit nonlinear traveling waves exist, but also traveling pulses, which carry a large dipole moment, and kink solutions are found, where the kinks describe the statics and dynamics of ferroelectric domain walls. More recently we have addressed the existence regimes of nonlinear periodic traveling waves, and their time and mass dependence.²³ It was shown that local structural anomalies as, e.g., observed in cuprate superconductors can be associated with these solutions. Most importantly it was shown that the observability of double-well potentials is crucially dependent on the time scale of the observation probe; this finding may help to clarify controversial experimental results about the existence of local double-well potentials inferred from new experimental techniques like pulsed neutron diffraction, the pair distribution function (PDF), NMR, and extended x-ray absorption fine structure (EXAFS). These techniques can all probe local structural features, but require investigation of time-dependent effects, as these experiments use a different time scale as compared to more conventional methods such as Raman, infrared, and inelastic neutron scattering techniques. Interestingly a molecular dynamics simulation of the two-dimensional version of the nonlinear shell model²⁴ also shows that there is a coexistence regime of two different time scales in the particle displacement which obey distinct dynamics.

Here we continue former investigations on the exact so-

lutions of the nonlinear polarizability model using the continuum approximation. Again time- and mass-dependent effects are investigated in addition to effects caused by anharmonicity and the potential barrier height. Instead of solving for nonlinear periodic wave solutions, we concentrate here on the existence regime of (pseudo)harmonic periodic waves with phonon-type character in order to explore the origin of anomalously large dipole moments and oscillator strengths observed in certain systems.

It should be mentioned that a huge amount of effort has been devoted to solving electron-phonon interaction models. These models are usually based on the Fröhlich²⁵ or Holstein model²⁶ for which it can be shown that double-well potentials in the phonon displacement coordinates can be generated by sufficiently strong electron-phonon coupling.²⁷ Also models combining inter- and intrasite electron-phonon couplings have been investigated in detail and ‘‘soliton’’ solutions carrying fractional charges have been discovered.²⁸ The possibility for structural instability has been included in a Peierls system by considering explicitly anharmonic mode-mode coupling, which crucially influences the order of the structural phase transition.²⁹ Models of these types find a variety of applications in quasi-one-dimensional crystals with a Peierls or spin-Peierls instability.^{30–32} Even though the nonlinear shell polarizability model is phenomenologically derived, it has a variety of features in common with the above-mentioned approaches as it represents in its quantum-mechanical analog an electron-phonon interaction model with on-site and intersite electron-phonon coupling and anharmonic lattice potentials^{33,34} similar to the case discussed in Ref. 29. But, in addition, electron-mediated mode-mode coupling is considered and multi-phonon-electron density interactions are obtained, which can model, e.g., *c*-axis-related effects in high- T_c superconductors.^{35–37}

The paper is organized in the following way: In the first section we introduce the model and briefly review results from earlier work. In the second section the effects of changing the double-well potential height on the dipole moment and the core and shell displacements are discussed together with the resulting displacement frequency spectra which reveal mode softening as expected for, e.g., ferroelectrics. It is also found that an ‘‘acoustic-mode’’-type dipole moment increases with decreasing frequency and huge oscillator strengths, incompatible with harmonic lattice dynamics, result. In the third, fourth, and fifth sections the same quantities as functions of anharmonicity, mass, and time are investigated. Increasing the anharmonicity up to the existence limit of pseudoharmonic periodic traveling waves yields strongly nonlinear but periodic waves for the individual core and shell motions, which show multiphonon contributions in the frequency spectrum and large oscillator strengths at high frequencies. Similar effects are also found with increasing mass ratio of the two sublattices, even though the mass ratio acts in a similar way on the effective potential as the barrier height. Beyond a certain critical mass ratio (pseudo)harmonic periodic waves no longer exist as the shape of the potential is reversed. As has been stressed recently in detail,²³ the time scale plays a very important role for particle dynamics. Here, huge optic-mode-type dipole moments develop in the low-velocity regime which are due to out-of-

phase motions of core and shell which admit for charge transfer or local ionization processes.

II. MODEL

The Hamiltonian of the nonlinear polarizability shell model in the diatomic linear chain version consists of a local on-site double-well potential in the relative core-shell displacement W with harmonic force constant g_2 and fourth-order constant g_4 , where the relative displacement refers to the difference in displacement coordinate U_1 of the core with mass m_1 and its surrounding shell with displacement coordinate $V_1 \triangleq V$. Mode-mode coupling is provided through the shells only with harmonic coupling f which couples the non-polarizable mass m_2 to the shells of m_1 . Lattice stability is provided through next-nearest-neighbor core-core coupling f' at m_1 . In the continuum limit the displacement coordinates are expanded with respect to time $\tau=2a/v$, where a is the lattice constant and v the phase velocity. The equations of motion using the adiabatic approximation for the shell motion read

$$m_1 \ddot{U}_{1n} = f' \tau^2 \ddot{U}_{1n} + g_2 W_{1n} + g_4 W_{1n}^3, \quad (1a)$$

$$m_2 (\ddot{U}_{2n} + \ddot{U}_{2n+1}) = -2g_2 W_{1n} - 2g_4 W_{1n}^3 + f \tau^2 \ddot{W}_{1n} + f \tau^2 \ddot{U}_{1n}, \quad (1b)$$

$$\ddot{U}_{2n} + \ddot{U}_{2n+1} = \frac{g_2}{f} \ddot{W}_{1n} + \frac{3g_4}{f} \ddot{W}_{1n} W_{1n}^2 + \frac{6g_4}{f} \dot{W}_{1n}^2 W_{1n} + 2\ddot{U}_{1n} + 2\ddot{W}_{1n}. \quad (1c)$$

The coupled equations (1) can be reduced to a single equation in $W_{1n} \equiv W$ which is of Bernoulli type, i.e.,

$$A \ddot{W} + B \ddot{W} W^2 + C W \dot{W}^2 + D W + E W^3 = 0, \quad (2)$$

with

$$A = 1 + \frac{m_2 g_2}{2M_2 f}, \quad (3a)$$

$$B = \frac{3g_4 m_2}{2M_2 f}, \quad (3b)$$

$$C = \frac{3g_4 m_2}{M_2 f}, \quad (3c)$$

$$D = g_2 \left(\frac{1}{M_1} + \frac{1}{M_2} \right), \quad (3d)$$

$$E = g_4 \left(\frac{1}{M_1} + \frac{1}{M_2} \right), \quad (3e)$$

and

$$M_1 = m_1 - f' \tau^2, \quad (4a)$$

$$M_2 = m_2 - \frac{f}{2} \tau^2, \quad (4b)$$

$$\frac{1}{M} = \frac{1}{M_1} + \frac{1}{M_2}. \quad (4c)$$

Equation (2) can be integrated and yields an effective potential in W (see Refs. 22, 23).

Slowly oscillating nonlinear periodic solutions exist for small v , which become standing periodic waves in the limit $v \rightarrow 0$. These types of solutions can be interpreted as modeling structural anomalies. If the particle dynamics are confined to a single well, traveling kink solutions are obtained which also exist in the static limit, where they correspond to ferroelectric domain walls. Large velocity solutions exist for certain values of the mass ratio and g_2 being positive and have either kink or pulse-exciton character. The pulse-exciton solutions, in particular, admit, in the static limit, local ionization processes or charge transfer processes which carry an integrated dipole moment. Huge polarization waves and large amounts of energy are associated with them, which might be important in understanding the dynamics of biomolecules.³⁸ Solutions which have been obtained in the lattice case exist also in the continuum limit, where besides the ferro- and antiferroelectric solutions, also commensurate periodic wave solutions are found with periods 3, 4, 5, and 6.

It is important to note that the solutions discussed above critically depend on the parameter regime and consequently have a restricted existence area. It should also be noted that they are not obtained, except for the first case discussed, by solving Eq. (2) directly, but by investigating the effective potential. In the following, Eq. (2) is, as in Ref. 23, solved exactly numerically. As has already been pointed out before, only harmonic periodic or quasiperiodic traveling-wave solutions are addressed as these can be interpreted in terms of phonon-type excitations. These solutions exist in certain parameter regimes only, which will be discussed below and obey all the same boundary conditions, i.e., maximum velocity at $W \equiv 0$. In no case are they really fully periodic and harmonic, due to the highly anharmonic character of the potential, but always only quasiperiodic and quasiharmonic. In addition, only waves are considered which cross the origin and have two equivalent (or nearly equivalent) turning points. The local on-site potential is in all investigated cases of ϕ_4 type, i.e., $g_2 < 0$, $g_4 > 0$, which, not necessarily, is true for the effective potential. Also we associate, in analogy to Ref. 22, with the relative core-shell displacement coordinate, an effective dipole moment as core and shell are oppositely charged. The origin of the dipole moment is then discussed in terms of individual core and shell displacements. In all cases investigated the harmonic next-nearest and second-nearest-neighbor couplings have been kept constant as well as the rigid mass m_2 and are the same throughout the paper (see Figs. 1–15).

III. VARIATION OF THE DOUBLE-WELL POTENTIAL DEPTH

The depth of the local double well is determined through g_2 which is taken as a variable in this section. As the structural transition temperature T_c is directly proportional to g_2 , increasing $|g_2|$ corresponds to an increase in T_c . The displacement-velocity dependence for various values of g_2 is shown in Fig. 1. For small g_2 the displacement at zero ve-

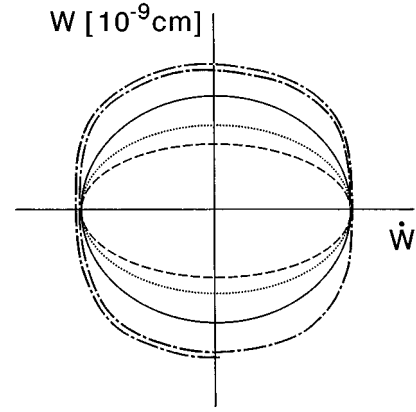


FIG. 1. Displacement-velocity dependence for $g_2 = -0.03$ (dashed-dotted line), -0.63 (solid line), -1.63 (dotted line), -2.63 (dashed line). All other parameters are given in Table I which are the same in all figures of Sec. III. g_2 is given in units of 10^4 erg cm^{-2} .

locity is large and decreases systematically with increasing $|g_2|$. g_2 being very small corresponds to the fact that the system is close to the phase transition where the anharmonicity dominates the dynamics. This is evident from Fig. 1 as the particle motion clearly starts deviating from quasiharmonic behavior to freeze in statically. Consequently W becomes a multivalued function of the velocity W corresponding to the increasing time. The multivalued solutions are in this case a consequence of the proximity to the phase transition, where nonlinear effects dominate the particle dynamics. With increasing $|g_2|$ the displacement-velocity dependence reveals strong amplitude reductions and increasing frequencies. This becomes more evident by examining at the time development of W (Fig. 2). It is clearly seen that the dynamics slow down when approaching the phase transition and huge increases in the oscillating dipole are observed, which can be associated with mode softening. With decreasing g_2 the dipole moment increases, and huge oscillator strengths are expected to be associated with low-frequency modes, while the frequency shifts to zero. The variation of the potential depth thus clearly simulates temperature effects on the system dynamics. The effective potential as a function of W and g_2 is shown in Fig. 3. Here the potential seems to be-

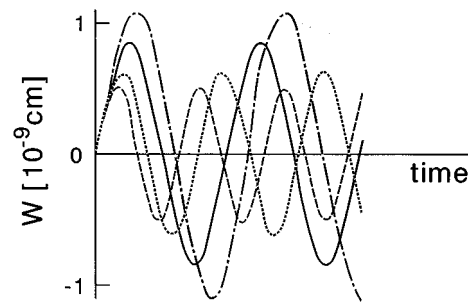


FIG. 2. Time dependence of the relative displacement W for $g_2 = -0.03$ (dashed-dotted line), -0.63 (solid line), -1.63 (dotted line), -2.63 (dashed line).

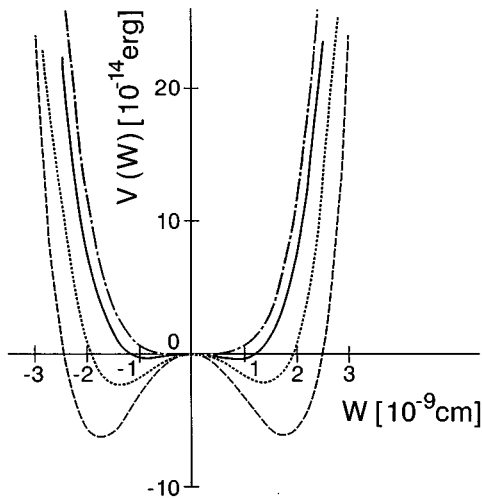


FIG. 3. Effective potential $V(W)$ as a function of W for $g_2 = -0.03$ (dashed-dotted line), -0.63 (solid line), -1.63 (dotted line), -2.63 (dashed line).

come infinitely large at finite W , but beyond the scale of Fig. 3 the potential reaches a maximum at $W = 0.65 \text{ \AA}$ for each g_2 and goes through zero again at $W = 0.79 \text{ \AA}$ to become infinitely negative. The height of the maximum varies nonlinearly with g_2 and reaches its largest value at $g_2 = -0.5$. In any case, the barrier height is larger than several thousands of eV's, which certainly confines the particle motion to oscillate within the barriers, but as the barrier width is only 0.14 \AA , it is possible that tunneling through the barriers may be observed under appropriate conditions. The origin of the huge dipole moments can be investigated by solving the equations of motion for U_1 and $V = U_1 + W \equiv$ shell displacement coordinate, separately. In Fig. 4 the time dependence of U_1 is shown. V exhibits the same time dependence as U_1 , but shows larger amplitudes for all values of g_2 . Note that

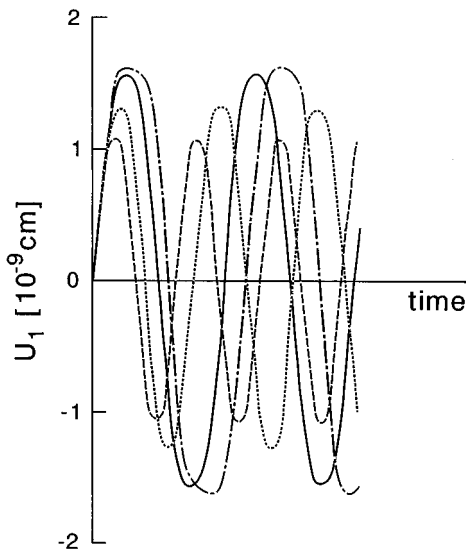


FIG. 4. Time dependence of the core displacement coordinate U_1 for $g_2 = -0.03$ (dashed-dotted line), -0.63 (solid line), -1.63 (dotted line), -2.63 (dashed line).

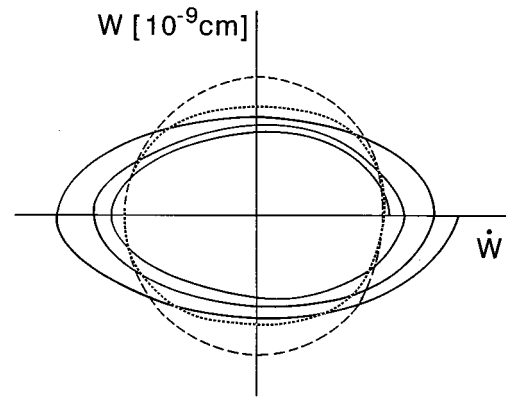


FIG. 5. Displacement-velocity dependence for $g_4 = 0.01$ (dashed line), 1.2 (dotted line), 5.0 (solid line). All other parameters are given in Table I and are the same in all figures of Sec. IV. g_4 is given in units of $10^{22} \text{ erg cm}^{-4}$.

the scale has changed as compared to Fig. 2. The amplitudes of both U_1 and V are much larger than of W . All displacement coordinates W , U_1 , and V show the same periodicity for the same g_2 and oscillate in phase. The dipole moment is thus only due to the different amplitudes of U_1 and V , and is termed ‘‘acoustic type’’ to emphasize the distinction from dipole moments originating from opposite displacements of U_1 and V . The displacement-frequency spectra of U_1 and V , as expected, reproduce mode softening of the system with decreasing $|g_2|$ and large displacements of both core and shell, associated with the lowest frequencies.

IV. VARIATION OF ANHARMONICITY

In this section the anharmonic core-shell coupling is varied and g_2 is kept constant (Table I). The displacement of W as a function of velocity is shown in Fig. 5. For small anharmonicity the particle dynamics is highly periodic and harmonic with large static displacements. Increasing g_4 reduces the static displacements but the motion is still nearly periodic and quasiharmonic. For $g_4 = 5$ the motion becomes highly nonlinear and the velocity as well as the displacement increases rapidly with increasing time. In this case W becomes, again similar to Fig. 1 and $g_2 = -0.03$, a multivalued function of the velocity due to the fact that strong anharmonicity dominates the dynamics and admits for new solutions with increasing time. It should be noted here that the system is not close to the phase transition, but the terms in Eq. (2) proportional to B , C , and E dominate the nonlinear dynamics. The stability limit to observe quasiperiodic traveling waves is reached for $g_4 = 45.0$, which corresponds to an extremely steep potential. The time development of W strongly resembles the previous case (Fig. 2) and it is not very apparent that the particle motion is no longer periodic. The increase in g_4 clearly yields faster traveling-wave solutions with decreasing amplitude. In the case of largest anharmonicity the amplitude of oscillations becomes strongly time dependent, i.e., increasing with increasing time. The displacement-frequency spectrum shows mode softening with decreasing g_4 , but large increases in the dipole moment with increasing g_4 . This means that high-frequency modes with large dipole moments can be associated with large anharmonicity. This

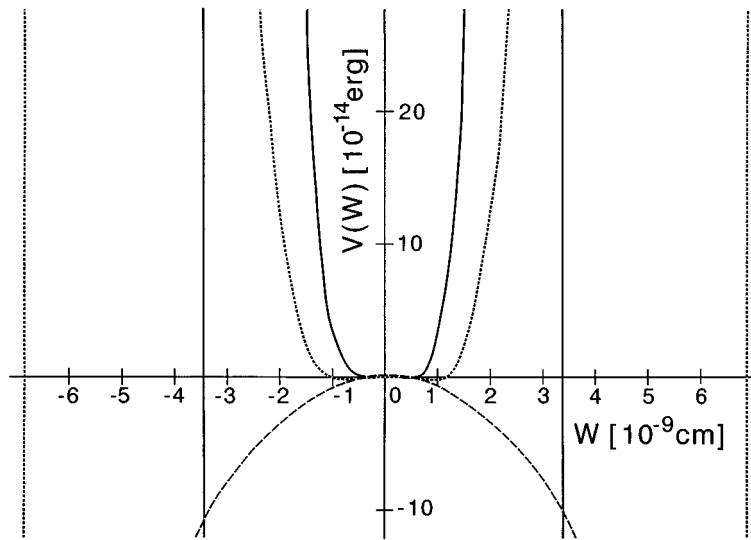


FIG. 6. Effective potential $V(W)$ as a function of W for $g_4=0.01$ (dashed line), 1.2 (dotted line), 5.0 (solid line).

result is certainly important for structurally stable systems with negligible mode softening, as, e.g., high- T_c superconductors, where very large oscillator strengths of certain lattice modes have been observed.^{39,40} The variation of the effective potential with g_4 is shown in Fig. 6. For the smallest g_4 ($=0.01$) the potential has deep broad double-well character (this is beyond the scope of the figure). With increasing g_4 the potential narrows and again seems to become unbounded at small W . But again it is found that the barrier is finite, the maximum now being dependent on g_4 , like the width of the barrier. With increasing g_4 the maximum shifts to smaller values of W and the width decreases rapidly, thus favoring tunneling through the barrier which would admit for huge W and charge transfer processes. The origin of the large dipole moments associated with high-frequency modes can be deduced from the individual core and shell displacements (Figs. 7 and 8). For very small g_4 slow oscillations of core and shell with moderate amplitudes are found, which are periodic but already strongly nonlinear. Also the individual displacements are out of phase but have the same periodicity. With increasing anharmonicity the core displacement becomes much smaller, strongly nonlinear, and clearly aperiodic while the shell displacement amplitude remains approximately the same for all g_4 and seems to be

pseudoharmonic and periodic. The frequency spectra of U_1 and V show for all values of g_4 multifrequency responses which shift to the higher-frequency side with increasing g_4 . With increasing g_4 the response of U_1 becomes smaller as compared to the very small anharmonicity case, while the opposite happens for the shell displacement. These large dipole moments observed for high frequencies originate from the large shell displacements; those displace opposite to the cores which behave highly anharmonic with very small amplitudes.

V. VARIATION OF THE MASS RATIO m_1/m_2

The mass ratio is varied by varying the polarizable sublattice mass. The double-well potential-defining parameters are kept constant and are given in Table I. The displacement velocity dependency is shown in Fig. 9. As should be expected the static displacement decreases, with increasing m_1 , being less than half as compared to the smallest mass. The time dependence of W is shown in Fig. 10. Interestingly and *opposite* to harmonic lattice dynamics, the heavy mass leads to rapid small amplitude oscillations in the dipole moment, which increase in amplitude but decrease in velocity with decreasing mass. The frequency spectrum in Fig. 11 shows mode softening with decreasing mass m_1 and large dipole

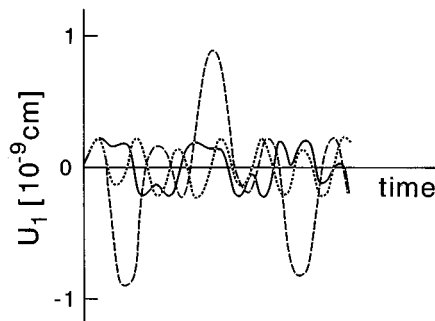


FIG. 7. Time dependence of the core displacement coordinate U_1 for $g_4=0.01$ (dashed line), 1.2 (dotted line), 5.0 (solid line).

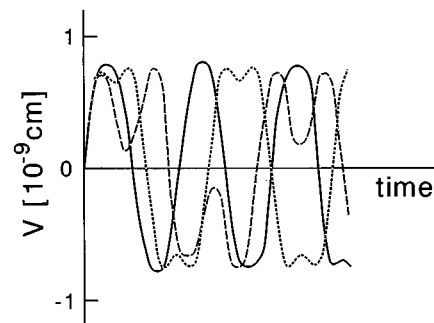


FIG. 8. Time dependence of the shell displacement coordinate V for $g_4=0.01$ (dashed line), 1.2 (dotted line), 5.0 (solid line).

TABLE I. Model parameters used in Sec. III.

$m_1 = 0.5 \times 10^{-22} \text{ g}^a$
$m_2 = 1.46 \times 10^{-22} \text{ g}$
$f = 14.41 \times 10^4 \text{ erg cm}^{-2}$
$f' = 1.27 \times 10^4 \text{ erg cm}^{-2}$
$g_2 = -0.63 \times 10^4 \text{ erg cm}^{-2},^b -2.63 \times 10^4 \text{ erg cm}^{-2}^c$
$g_4 = 0.904 \times 10^{22} \text{ erg cm}^{-4}^d$
$\tau = 1 \text{ THz}^{-1}^e$

^aUsed in Figs. 1, 5, and 15.

^bUsed in Fig. 5 only.

^cUsed in Figs. 9 and 15.

^dUsed in Figs. 1, 9, and 15.

^eUsed in Figs. 1, 5, and 9.

moments associated with low-frequency modes. For the largest mass m_1 multiphonon contributions are observed, indicating that the system becomes more anharmonic if the polarizable sublattice mass is increased. Altogether the dipole moment is rather small as compared to the previously investigated cases. This is due (Fig. 12) to the fact that core and shell displacements are in phase, both being extremely large (note that the scale has changed), but of the same order of magnitude, thus nearly leading to cancellations. The frequency spectrum for U_1 (Fig. 13) also shows mode softening with increasing mass, but very large displacement contributions at various frequencies with increasing mass underlining the increasing anharmonicity. The shell displacement and the shell displacement frequency spectrum are very similar to the corresponding core dynamics, as already outlined above (see Figs. 12 and 13) and have been omitted here. The mass dependence of the effective potential (Fig. 14) shows that the decrease in mass m_1 deepens the potential wells drastically and steepens the potential which corresponds to increasing anharmonicity. The stability limit for quasiharmonic periodic waves is reached when the two sublattice masses are approximately the same. This case is especially interesting for observing nonlinear traveling waves where huge dipole moments have been found. Beyond the stability limit of the quasiharmonic solutions, i.e., $m_1 > m_2$, the potential shape reverses (see Fig. 14) and the wells decrease with increasing mass. Note that also here the height is not infinite but mass dependent and of the order of several hundred eV's. The

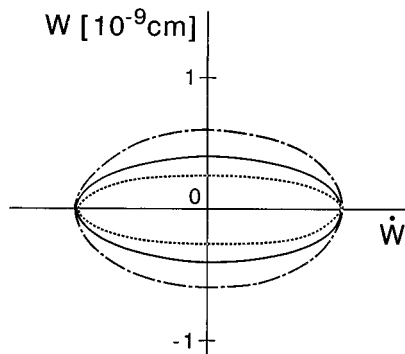


FIG. 9. Displacement-velocity dependence for $m_1=0.2$ (dashed-dotted line), 0.8 (solid line), 1.1 (dotted line). All other parameters are given in Table I and are the same in all figures of Sec. V. m_1 is given in units of 10^{-22} g .

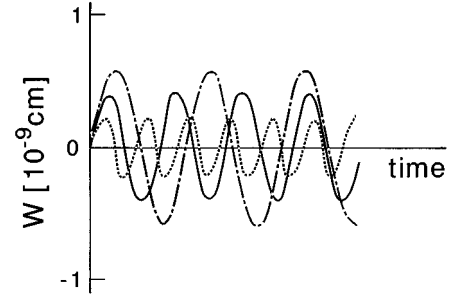


FIG. 10. Time dependence of the relative displacement coordinate W for $m_1=0.2$ (dashed-dotted line), 0.8 (solid line), 1.1 (dotted line).

same holds for the minima when $m_1 > m_2$. As the variation of masses mainly reflects itself in a change of the potential barrier it should consequently lead to a change in the structural phase transition temperature when a system is alloyed, diluted, or mixed with another system. For instance, in $\text{KTa}_{1-x}\text{Nb}_x\text{O}_3$ it is observed that T_c systematically increases with increasing x (see, e.g., Ref. 8). As in the present model m_1 refers to the polarizable cluster BO_3 of ABO_3 perovskites, the large increases in T_c are readily attributable to the mass differences of Ta and Nb ions and obey the finding from the model calculations. Note that this coincides with frozen-phonon local density approximation (LDA) calculations where a smooth double well is observed for pure KTaO_3 and a deep double well for KNbO_3 .^{41,42} Also in $\text{La}_{1-x}\text{Sr}_x\text{CuO}_4$ the above rule is obeyed where in this case the mass ratio is varied by changing m_2 . With increasing La content, i.e., decreasing m_1/m_2 , T_c , which corresponds to the structural transition temperature, increases.⁴³⁻⁴⁶ The consequences from the importance of the mass ratio on T_c could experimentally be used in optimizing material properties for specific applications. As the potential barriers are very high and their width being much larger than observed in the variation of g_4 , it is unlikely that tunneling and strongly nonlinear solutions are obtained if the critical ratio is not exceeded. Note that the mass ratio also plays a crucial role to observe order-disorder, displacive transitions.⁴⁷

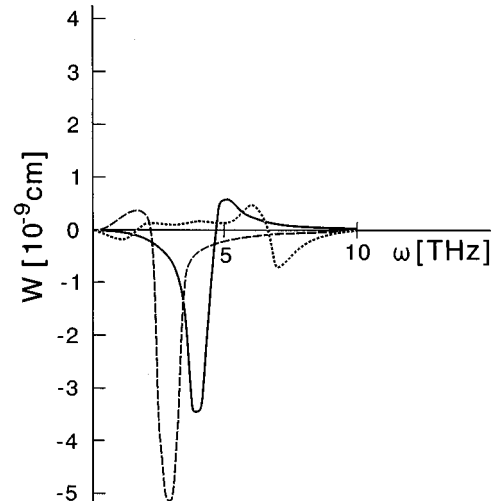


FIG. 11. Displacement-frequency dependence $W(\omega)$ for $m_1=0.2$ (dashed line), 0.8 (solid line), 1.1 (dotted line).

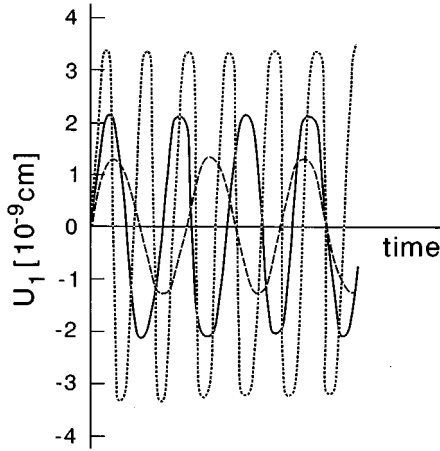


FIG. 12. Time dependence of the core displacement coordinate U_1 for $m_1=0.2$ (dashed line), 0.8 (solid line), 1.1 (dotted line).

VI. TIME-DEPENDENT EFFECTS

The time dependence has been addressed recently already²³ by solving Eq. (2) for nonlinear traveling-wave solutions. The critical influence of the time scale has been emphasized in detail and we continue this former work by including here time effects on phonon-type solutions. The displacement-velocity dependence is shown in Fig. 15. While on the phonon time scale moderate static dipole moments are observed large increases are obtained with increasing time. This becomes more obvious from Fig. 16 where the traveling waves are shown as a function of time. While the expected fast velocity solutions exist for τ small, they dramatically slow down with increasing τ and show large increases in the amplitudes. The corresponding frequency spectrum (Fig. 17) shows huge dipole moments at zero frequency for large times. With decreasing time these are still present but a response at the optic mode emerges at higher frequency. For small τ only a moderate dipole moment is observed which could also be caused by ordinary optic-phonon modes. The reason for the huge increases in dipole

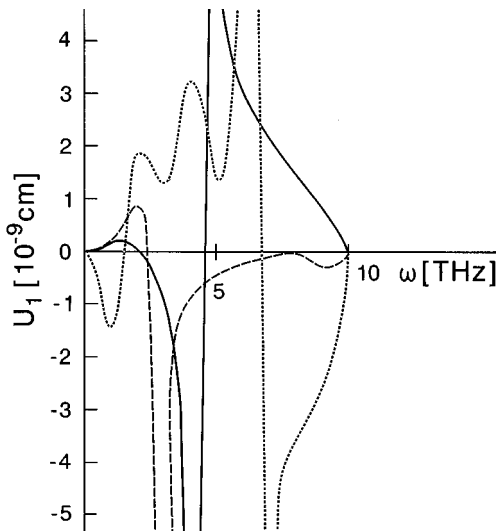


FIG. 13. Displacement-frequency dependence $U_1(\omega)$ for $m_1=0.2$ (dashed line), 0.8 (solid line), 1.1 (dotted line).

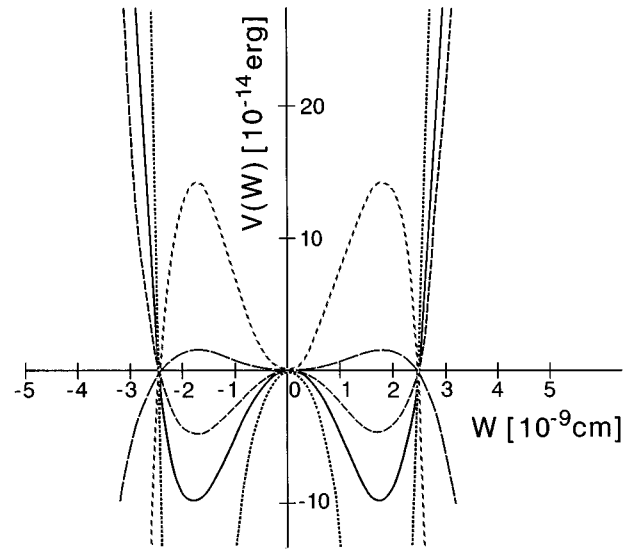


FIG. 14. Effective potential $V(\omega)$ as a function of W for $m_1=0.2$ (dashed line), 0.8 (solid line), 1.1 (dotted line), 1.55 (reversed potential, dashed line), 3.1 (long-dashed line).

moment becomes clear from investigating the individual displacements of core and shell. For τ small core and shell displace in phase, both being of the same order of magnitude. With decreasing velocity they displace in opposite directions where specifically the shell displacement becomes very large indicating charge transfer or local ionization processes (Figs. 18 and 19). Simultaneously the dynamics is no longer quasiharmonic but becomes increasingly nonlinear

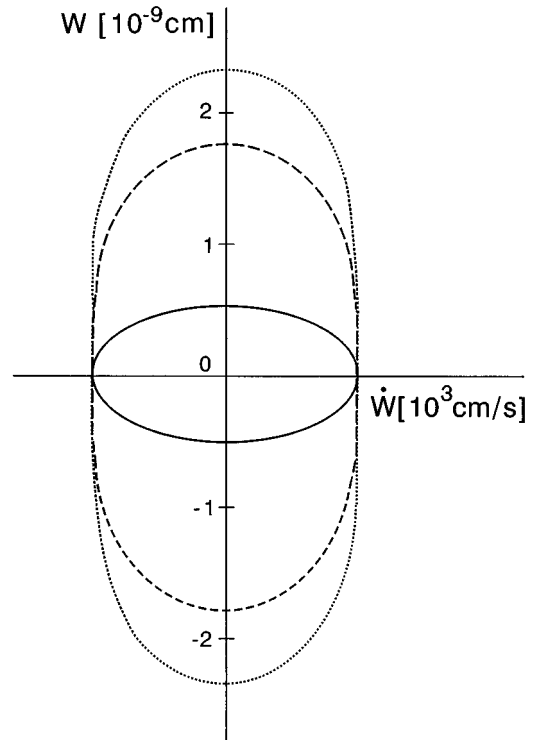


FIG. 15. Displacement-velocity dependence for $\tau=0.75$ (solid line), 2.5 (dashed line), 4 (dotted line). All other parameters are the same in all figures of Sec. VI and are given in Table I. τ is given in units of THz^{-1} .

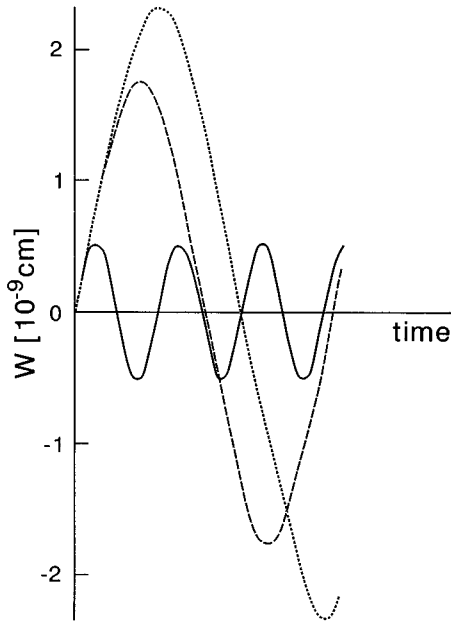


FIG. 16. Time dependence of the relative displacement coordinate W for $\tau=0.75$ (solid line), 2.5 (dashed line), 4 (dotted line).

and slows down significantly. The frequency spectrum of U_1 and V shows moderate responses in the high-velocity regime for both U_1 and V . With decreasing velocity a static component develops which is huge for the shell displacement but of moderate values for the core displacement coordinate. While at intermediate τ a response of the system at the original frequency is still observed, this vanishes nearly completely in the static case. The time dependence of the potential is shown in Fig. 20. In the static and intermediate velocity case a broad single minimum potential is observed which narrows with increasing velocity and develops gradually double-well

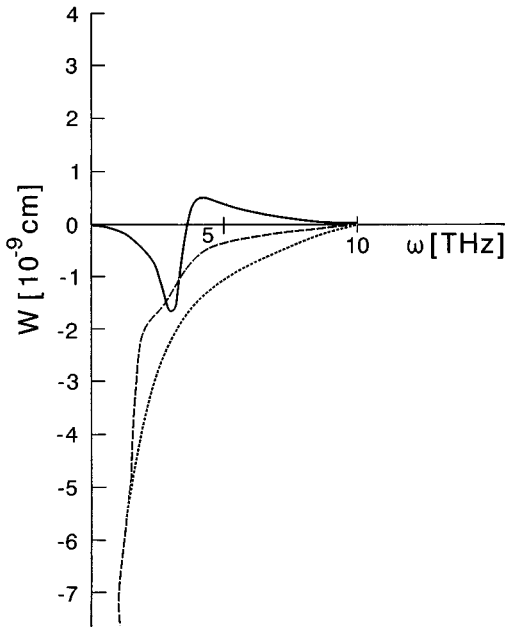


FIG. 17. Displacement-frequency dependence $W(\omega)$ for $\tau=0.75$ (solid line), 2.5 (dashed line), 4 (dotted line).

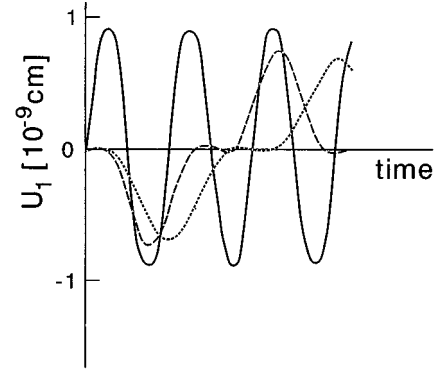


FIG. 18. Time dependence of the core displacement coordinate U_1 for $\tau=0.75$ (solid line), 2.5 (dashed line), 4 (dotted line).

character. Again, as previously, the potential is not infinitely high but has a maximum which has a τ -dependent height and width at τ -dependent values of W . The stability limit to observe pseudoharmonic periodic traveling waves is reached for $\tau=0.6 \times 10^{-12}$ s, where the potential reverses shape and develops deep minima beyond $W=0.15$ Å. Fast kink and pulse solutions exist in this regime, which have been discussed in Ref. 22. The time scale clearly influences the dynamics in a crucial way, as the development of local double-well potentials critically depends on it.

VII. CONCLUSIONS

We have carried out a systematic investigation of particle dynamics in anharmonic potentials arising in a one-dimensional nonlinear shell model. The boundary conditions and the parameter space have been chosen such as to admit for (pseudo) harmonic pseudoperiodic traveling-wave solutions only. These solutions are of special interest as phonon-type excitations can be associated with them, and the dependence of oscillator strengths on the model parameters can be obtained. It is found that changing the double-well potential barrier height reproduces the soft mode behavior observed in ferrodistortive structural phase transitions. With decreasing

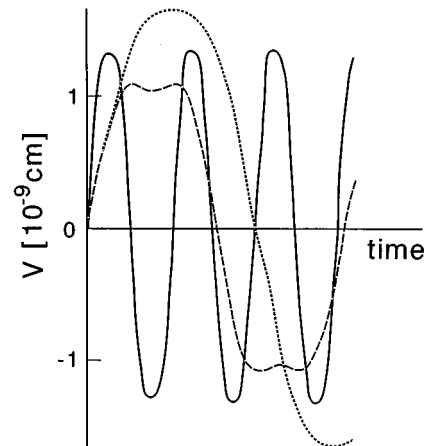


FIG. 19. Time dependence of the shell displacement coordinate V for $\tau=0.75$ (solid line), 2.5 (dashed line), 4 (dotted line).

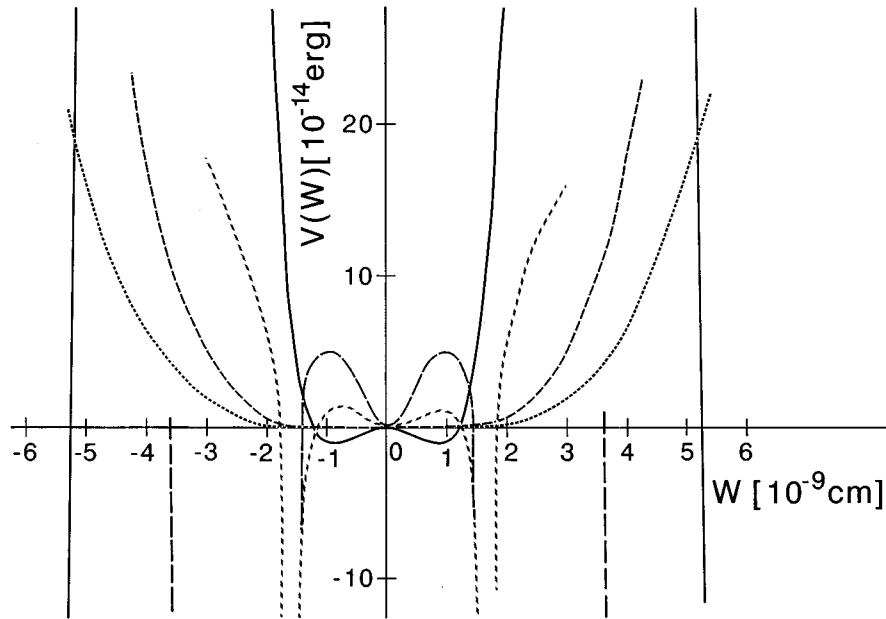


FIG. 20. Effective potential $V(W)$ as a function of W for $\tau=0.75$ (solid line), 2.5 (dashed line), 4 (dotted line), 0.5 (broken dashed line), 0.6 (long-dashed line).

height the frequency decreases and simultaneously an increase in the dipole moment is observed, which corresponds to increasing oscillator strengths and large effective charges. It should be mentioned here that the high effective charges associated with soft modes in ferroelectrics have also been addressed in Refs. 48, 49 and were ascribed to the strong anharmonicity of these systems. From the present analysis we conclude that the anharmonicity does not lead to large effective charges for low-frequency modes, but the attractive harmonic interaction causes the huge oscillator strengths associated with these modes.

The large dipole moments at low frequencies result from the in-phase motion of core and shell; i.e., they are of ‘‘acoustic type,’’ where the large difference in the respective displacements causes the net effective moment. Both core and shell show anomalously large displacements with decreasing barrier height, as compared to the other cases which we investigated.

The variation of the anharmonicity of the potential shows that with increasing anharmonicity the dipole response shifts to higher frequencies and huge effective charges, i.e., oscillator strengths, are observed at high frequencies. This observation is certainly relevant for systems which are structurally stable but show anomalously large oscillator strengths incompatible with harmonic lattice dynamics. From the present investigation we conclude that strong anharmonicity favors such findings. The reason for the development of large dipole moments with increasing anharmonicity is the out-of-phase motion of core and shell, where the core displacement is confined to strongly anharmonic small amplitude motions in the steep potential, whereas the shell undergoes large amplitude displacements. For both core and shell, multiphonon responses are observed. As the outer potential barrier width rapidly decreases with increasing g_4 , tunneling processes are possible which could lead to charge transfer and local ionization processes. Also highly nonlinear nonperiodic solu-

tions are to be expected to exist beyond the barriers, corresponding to exciton-type solutions.

The change in the mass ratio of polarizable to rigid ion mass shows unusual features as, opposite to harmonic cases, mode softening with increasing dipole moment is observed for decreasing mass m_1 . The net dipole moment results, as in the case of changing the barrier height, from the in-phase displacements of core and shell, where both are large but the shell displacement being substantially larger than the core displacement. With increasing mass broad and strong multiphonon contributions are obtained for the core as well as the shell displacement. The effective potential reverses its shape at a critical mass ratio where both masses are approximately the same. The mass dependence of the dipole frequency response is important in understanding the large changes in the ferroelectric phase transition temperature when substituting the transition metal in oxide perovskite or the cation sublattice. From the present analysis it is predicted that T_c increases with decreasing ratio m_1/m_2 (note that m_1 refers to the polarizable cluster, transition metal surrounded by the oxygen octahedra in perovskite, while m_2 represents the rigid cations). In a previous analysis it is found, in addition, that simultaneously order-disorder effects become dominantly more important.⁴⁷

The importance of the time scale on the particle dynamics has already been addressed recently.²³ In accordance with former findings we have shown here that the observation of double-well potentials crucially depends on the time scale. In the static case, broad single-well potentials are observed whereas in the high-velocity regime narrow double wells appear. Experimentally this should be important with respect to measurements of the Debye-Waller factor, for instance, which tests the ‘‘static limit’’ or EXAFS results which are in the high-velocity regime. Clearly different results should be obtained from both experiments probing the same sample.

Further, the development of large dipole moments with decreasing velocity is observed which in the static limit are reminiscent of charge transfer processes. These large dipole moments are of “optic type” and result from the out-of-

phase motion of core and shell. Even though the shell model is phenomenologically based, anomalous experimental observations, specifically with respect to unusual large oscillator strengths, can be interpreted consistently.

- ¹R. Migoni, H. Bilz, and D. Bäuerle, *Phys. Rev. Lett.* **37**, 1155 (1976).
- ²R. Migoni, Ph.D. thesis, University of Stuttgart, 1976.
- ³H. Bilz, A. Bussmann, G. Benedek, H. Büttner, and D. Strauch, *Ferroelectrics* **25**, 339 (1980).
- ⁴H. Bilz, G. Benedek, and A. Bussmann-Holder, *Phys. Rev. B* **35**, 4840 (1987).
- ⁵C. Perry, R. Currat, H. Buhay, R. Migoni, W. Stirling, and J. Axe, *Phys. Rev. B* **39**, 8666 (1989).
- ⁶R. L. Migoni, K. H. Rieder, K. Fisher, and H. Bilz, *Ferroelectrics* **13**, 377 (1976).
- ⁷D. Khatib, R. L. Migoni, G. E. Kugel, and L. Godefroy, *J. Phys. Condens. Matter* **1**, 9811 (1991).
- ⁸G. E. Kugel, M. D. Fontana, and W. Kress, *Phys. Rev. B* **35**, 813 (1987).
- ⁹M. Stachiotti and R. Migoni, *J. Phys. Condens. Matter* **2**, 4341 (1990).
- ¹⁰M. Stachiotti, R. Migoni, and U. Höchli, *J. Phys. Condens. Matter* **3**, 3689 (1991).
- ¹¹A. Bussmann-Holder, H. Bilz, and G. Benedek, *Phys. Rev. B* **39**, 9214 (1989).
- ¹²A. Bussmann-Holder and H. Bilz, *Ferroelectrics* **54**, 5 (1984).
- ¹³A. Bussmann-Holder and H. Büttner, *Ferroelectrics* **80**, 297 (1988).
- ¹⁴A. Bussmann-Holder, H. Bilz, and P. Vogel, in *Electronic and Dynamical Properties of IV-VI Compounds*, Vol. 99 of *Springer Tracts in Modern Physics*, edited by G. Höhler (Springer-Verlag, Berlin, 1983).
- ¹⁵A. Bussmann, H. Bilz, R. Roenspiess, and K. Schwarz, *Ferroelectrics* **25**, 343 (1980).
- ¹⁶R. E. Cohen and H. Krakauer, *Phys. Rev. B* **42**, 6416 (1990).
- ¹⁷For a recent review see, e.g., Proceedings of the “International Workshop of Fundamental Properties of Ferroelectrics,” Williamsburg, 1994/1995 [*Ferroelectrics* (to be published)].
- ¹⁸See e.g., F. Calogero, in *Statics and Dynamics of Nonlinear Systems*, edited by G. Benedek, H. Bilz, R. Zeyher (Springer-Verlag, Heidelberg, 1983), p. 7; F. Calogero and A. Degasperis, *Spectral Transform and Solitons: Tools to Solve and Investigate Nonlinear Evolution Equations* (North-Holland, Amsterdam, 1982), Vols. 1 and 2.
- ¹⁹H. Bilz, H. Büttner, A. Bussmann-Holder, W. Kress, and U. Schröder, *Phys. Rev. Lett.* **48**, 264 (1982).
- ²⁰H. Büttner and H. Bilz, *J. Phys. (Paris) Colloq.* **42**, C6-111 (1981).
- ²¹H. Büttner and H. Bilz, in *Recent Developments in Condensed Matter Physics*, edited by J. T. Devreese (Plenum, New York, 1981), Vol. 1.
- ²²G. Benedek, A. Bussmann-Holder, and H. Bilz, *Phys. Rev. B* **36**, 630 (1987).
- ²³A. Bussmann-Holder and A. R. Bishop, *Philos. Mag. B* (to be published); A. Bussmann-Holder, *J. Phys. Solids* (to be published).
- ²⁴M. Stachiotti, A. Dobry, R. Migoni, and A. Bussmann-Holder, *Phys. Rev. B* **47**, 2473 (1993).
- ²⁵H. Fröhlich, *Proc. R. Soc. London A* **223**, 296 (1954).
- ²⁶T. Holstein, *Ann. Phys.* **7**, 343 (1959).
- ²⁷C. C. Yu and P. W. Anderson, *Phys. Rev. B* **29**, 6165 (1984).
- ²⁸S. Kivelson, *Phys. Rev. B* **28**, 2653 (1983).
- ²⁹Y. Lepine, *Phys. Rev. B* **28**, 2659 (1983).
- ³⁰A. J. Berlinsky, *Rep. Prog. Phys.* **42**, 1243 (1979).
- ³¹J. W. Bray, L. V. Interrante, I. S. Jacobs, and J. C. Bonner, in *Extended Linear Chain Compounds*, edited by J. S. Miller (Plenum, New York, 1983), Vol. III, p. 353.
- ³²G. A. Toombs, *Phys. Rev.* **40**, 181 (1978).
- ³³A. Bussmann-Holder and A. R. Bishop, *Phys. Rev. B* **44**, 2853 (1991).
- ³⁴A. Bussmann-Holder, A. R. Bishop, and A. Simon, *Z. Phys. B* **20**, 183 (1993).
- ³⁵Z. Tešanović, A. R. Bishop, and R. L. Martin, *Solid State Commun.* **68**, 337 (1988).
- ³⁶A. Bussmann-Holder and A. R. Bishop, *Phys. Rev. B* **51**, 3460 (1995).
- ³⁷A. Bussmann-Holder and A. R. Bishop, *Phys. Rev. B* **51**, 6640 (1995).
- ³⁸H. Bilz, H. Büttner, and H. Fröhlich, *Z. Naturforsch.* **366**, 208 (1981).
- ³⁹See, e.g., M. Reedyk, T. Timusk, J. S. Xue, and J. E. Greedan, *Phys. Rev. B* **49**, 15 984 (1994) and references therein.
- ⁴⁰M. Sepiarsky, M. G. Stachiotti, and R. L. Migoni (unpublished).
- ⁴¹P. Böni, J. D. Axe, G. Shirane, R. J. Birgenau, D. R. Gabbe, H. P. Jenssen, M. A. Kastner, C. Y. Peters, P. J. Picone, and T. R. Thurston, *Phys. Rev. B* **38**, 185 (1988).
- ⁴²A. Migliori, W. M. Vissher, S. Wong, S. E. Brown, S. Tanaka, H. Kojima, and P. B. Allen, *Phys. Rev. Lett.* **64**, 2458 (1990).
- ⁴³S. W. Cheong, J. D. Thompson, and Z. Fisk, *Physica (Amsterdam)* **158C**, 109 (1989).
- ⁴⁴A. Bussmann-Holder, A. Miglioni, Z. Fisk, J. L. Sarrao, R. G. Leisure, and S.-W. Cheong, *Phys. Rev. Lett.* **67**, 512 (1991).
- ⁴⁵A. Bussmann-Holder, *J. Phys. Chem. Solids* (to be published).
- ⁴⁶P. B. Littlewood, *J. Phys. C* **13**, 4893 (1980).
- ⁴⁷V. Heine and P. B. Littlewood, *J. Phys. C* **12**, 4431 (1979).